Brown carbon aerosol formation by multiphase catechol photooxidation in the presence of soluble iron

David de Haan, Lelia Hawkins, Jacob Weber, Benjamin Moul, Samson Hui, Santeh Cox, Jennifer Esse, Nathan Skochdopole, Carys Lynch, Audrey de Haan, et al.

Brown carbon aerosol formation by multiphase catechol photooxidation in the presence of soluble iron

David O. De Haan,[1] Lelia N. Hawkins,[2] Jacob A. Weber,[2] Benjamin T. Moul,[2] Samson Hui,[1] Santeh A. Cox,[1] Jennifer U. Esse,[1] Nathan R. Skochdopole,[1] Carys P. Lynch,[1] Audrey C. De Haan,[1] Chen Le,[1] Mathieu Cazaunau,[3] Antonin Bergé,[4] Edouard Pangui,[3] Johannes Heuser,[3] Jean-François Doussin,[3] Bénédicte Picquet-Varrault[3]*

[1] Department of Chemistry and Biochemistry, University of San Diego, 5998 Alcala Park, San Diego CA 92110 USA

[2] Hixon Center for Climate and the Environment, Harvey Mudd College, 301 Platt Blvd, Claremont CA 91711 USA

[3] Université Paris-Est Créteil and Université Paris Cité, CNRS, LISA, F-94010 Créteil, France

[4] Université Paris Cité and Université Paris-Est Créteil, CNRS, LISA, F-75013 Paris, France

*Email: ddehaan@sandiego.edu

KEYWORDS. Fenton, surface activity, aqueous processing, smoke plume, photochemistry, secondary organic aerosol.

ABSTRACT

Catechol (*1,2*-benzenediol), a common phenolic species emitted during biomass burning, is both redox active and metal chelating. When oxidized by OH radicals in the aqueous phase, it rapidly forms brown carbon (BrC). Here, we report chamber studies of the multiphase chemistry of catechol using HOOH as an OH radical source, soluble iron, simulated sunlight, and either deliquesced or solid-phase seed particles. BrC of remarkable similarity (MAC_{365} = 1.7 ±0.2 m^2 g^{-1}, "medium-BrC" category) was produced whenever gas-phase catechol was photolyzed in the chamber, with or without the presence of an OH radical source, soluble iron, or deliquesced aerosol. The speed and quantity of BrC formation varied, however. While BrC production was slower in the absence of an OH radical source, multiple lines of evidence suggest that OH generation via photosensitization by surface-adsorbed catechol can still generate BrC. Fenton chemistry actively occurred in surface-adsorbed water layers even below the seed particle deliquescence point, leading to significant production of gas-phase benzoquinone. Ratios of BrC and secondary organic aerosol (SOA) relative to catechol concentrations were highest in the presence of trace amounts of soluble iron, HOOH, and simulated sunlight, indicating that photo-Fenton chemistry contributed substantially to BrC and SOA formation by catechol. Finally, we observed that BrC and SOA formation by catechol / photo-Fenton chemistry can occur efficiently even at 40% RH. These results are consistent with catechol being a major source of secondary BrC in biomass burning plumes, even at moderate relative humidity.

Synopsis

Photolysis and photooxidation of catechol, present in wood smoke, form similar brown carbon aerosol under varied environmental conditions (≥40% RH). Iron and an OH radical source enhance yields of brown carbon.

Introduction

Phenolic species are produced by lignin breakdown, are significant gas phase emissions from biomass burning, and are dominant secondary organic aerosol (SOA) precursors during plume aging.[1] Once absorbed into cloud droplets or aqueous aerosol particles, phenolic species can react with OH radicals[2] or triplet carbon species[3] to generate brown carbon (BrC) oligomer species.[4, 5] More substituted phenols reacting with triplet carbon generate the most light-absorbing BrC.[6] Catechol (*1,2*-benzenediol), an abundant phenolic species in smoke, is depleted from the gas phase within an hour of plume aging,[7] making it one of the most reactive organic components of smoke. It is both redox active (like other hydroxy phenols, forming semiquinone radicals and quinones) and metal chelating (because of its adjacent OH groups).[8] Thus, its atmospheric chemistry is expected to be closely tied to metals, such as iron, that are also present in clouds and aqueous aerosol due to the presence of dust and anthropogenic emissions. Catechol – Fe^{3+} coordination bonds are extremely strong at high pH (above catechol's pK_{a1} of 9.46), while at low pH iron promotes catechol oligomerization through redox activity.[9] Indeed, dark reaction between catechol and Fe^{3+} have been shown to form black, insoluble polymers in aqueous solution at pH 3.[10] As a redox-active ligand, catechol and the metal it is bound to can change oxidation states in a synergistic fashion ("valence tautomerism"),[11] opening up unusual reactive pathways while

creating ambiguity about the electronic states of catechol and the metal.[8] Catechol oxidation and Fe^{3+} reduction occur at similar potential, further linking their redox chemistry, such that aqueous Fe^{2+} / Fe^{3+} ratios depend on catechol concentrations in addition to pH and dissolved oxygen levels.[12] Coupled catechol-metal redox chemistry can also form persistent free radical species upon photolysis.[13]

Catechol can be oxidized in the gas phase, where rate constants for its reactions with •OH and ozone are $1.0 \pm 0.2 \times 10^{-10}$ cm^3 s^{-1} [14] and $13.5 \pm 1.1 \times 10^{-18}$ cm^3 s^{-1},[15] respectively, or in the aqueous phase, where its rate constants are 4.7×10^9 M^{-1} s^{-1} [16] and 3.1×10^5 M^{-1} s^{-1},[17, 18] respectively. Furthermore, catechol is a surface active species, making it susceptible to oxidation by gas-phase oxidants even after it is taken up by clouds or aqueous aerosol particles.[19] Taking these pathways into consideration, degradation of catechol in clouds by ozone, $•HO_2/•O_2^-$ and •OH has been estimated to account for 58.9%, 33%, and 1.2%, respectively, of the total daytime catechol sink in the atmospheric multiphase system, while gas phase reaction with •OH accounted for 6.1%, and biodegradation accounted for only 1.5% of daytime catechol losses.[17] Finally, once catechol is oxidized, the semiquinone radical and quinone products efficiently oligomerize into complex, light-absorbing structures.[20, 21]

In this work, we studied BrC and SOA formation during chamber photooxidation of gas-phase catechol in the presence of cloud droplets, aqueous aerosol, or solid aerosol seed particles, both with and without HOOH as an OH precursor, and both with and without the presence of iron, in order to better understand the multiphase interplay between catechol, dissolved iron, and oxidant species. We find that the quantity and speed of BrC and SOA formation was accelerated by the presence of dissolved iron and/or HOOH, while the nature of the BrC and SOA formed from catechol under illumination was remarkably similar under all conditions.

Materials and Methods

Experiments were performed in CESAM, a 4.2 m^3 temperature- and pressure-controlled steel smog/cloud chamber designed for studies of multiphase chemistry.[22] Gas-phase contents of the chamber during each experiment were monitored by a CO/CO_2 monitor, pressure, temperature, relative humidity (RH), and dilution flow sensors, proton transfer reaction mass spectrometry (PTR-ToF-MS, KORE II, 1-min. averaging), and long-path Fourier transform infrared (FTIR) spectroscopy (Bruker Tensor 37, 184 m pathlength, 0.5 cm^{-1} resolution, 5-min. averaging). FTIR data was analyzed by fitting to standard spectra using ANIR software, available from the Eurochamp data center. PTR-ToF-MS ion peaks were mass-calibrated and integrated using Grams software, and dilution-corrected using in-house *R* code.

Chamber aerosol and cloud droplet size distributions were monitored by scanning mobility particle sizing (SMPS, TSI 3080 / 3772, 3-min. averaging, sampling through a Nafion drying tube) and a droplet spectrometer (Palas welas, 0.4 to 15 μm range, 1-min. avg), respectively. SMPS aerosol number and mass data (assuming unit density) were corrected for the effects of gradual dilution and size-dependent wall losses in the chamber. The simple assumption of unit density was used in interpreting SMPS data because aerosol density was expected to change during each experiment as SOA was formed on inorganic seed particles, and these time-dependent densities were not measured. Aerosol optical properties were quantified by a 7-wavelength dual-spot aethalometer (Magee AE33, both 1-min.). Angstrom absorption exponents (AAE) were fit to the 6 aethalometer wavelengths between 470 to 950 nm. Optical properties of the water-soluble aerosol fraction were quantified by particle-into-liquid sampling (PILS) / waveguide absorbance spectrometry (2m path length, 1-min avg). Aerosol chemistry was probed via an aerosol chemical

speciation monitor (ACSM, Aerodyne, 6-min. avg, sampling through a Nafion drying tube). BrC mass absorption coefficients (MAC, in $m^2\ g^{-1}$) were calculated from PILS-waveguide absorption measured at 365 nm, using the equation

$$MAC_{365} = \frac{Abs_{365}}{bC\left(\frac{V_{sampled}}{V_{output}}\right)}$$

where Abs_{365} is the measured *ln*-based absorption at 365 nm, b is the waveguide optical path length, C is the organic aerosol concentration measured by ACSM in $g\ m^{-3}$, $V_{sampled}$ is the gas flow rate of PILS sampling from the chamber (7500 mL min^{-1}), and V_{output} is the PILS liquid outflow rate (0.33 to 0.50 mL min^{-1}).

Experiment conditions are summarized in Table 1. In a typical experiment, the chamber was filled with 80/20 N_2/O_2 to 4 mbar above ambient pressure, and all instruments were connected to the chamber for blank readings. After this, 100 ppb butanol-*d9* (for quantifying OH radicals from its loss)[23] and ~100 μg/m^3 seed particles were added, generated from solutions containing 10 mM sodium hydrogen sulfate ($NaHSO_4$, Sigma >90%) and, in Experiments 1 and 4-7, also containing 67 μM iron(II) sulfate ($FeSO_4$, Prolabo, >98%), such that the $NaHSO_4$ / $FeSO_4$ mole ratio was 150:1 in all experiments involving iron-containing seeds. Within 90 min., seed particle coagulation produced aerosol size distributions with relatively stable geometric mean diameters between 93 and 103 nm. Catechol vapor was injected into the chamber by heating catechol powder to 100 – 110ºC in a 2 L/min N_2 flow, a method that produced catechol concentrations that varied from run to run by approximately a factor or ±2. In Experiments 1b and 2, higher catechol concentrations were quantified in the chamber using long-path FTIR spectroscopy and ANIR spectral fitting to a standard gas-phase spectrum from the Eurochamp database.[24] This absolute quantitation was then used to calibrate PTR-MS catechol ion signals at *m/z* 111. HOOH(g) was

added in Experiments 3, 4, and 6 by bubbling a 2 L/min flow of N_2 through a 30% HOOH solution. Chamber humidity was increased in all experiments from < 5% to 40-42% RH (below $NaHSO_4$'s deliquescence point of 52% RH),[25] and then in Experiments 1-5 to 74 to 95% RH (well above the deliquescence point). The chamber was then illuminated by three 6500 W solar-simulator Xe arc lamps for 60-90 minutes. Each lamp is attenuated with a 6 mm thick pyrex plate to closely match the shortwave edge of the ground-level solar spectrum.[22]

Table 1. Summary of conditions for catechol photolysis and photooxidation chamber experiments.

Expt.	Fig.	Seed aerosol [a]	RH_{max} (%)	$[Catec.]_{peak}$ (ppb)	HOOH added (min.)	Lights on (min.)	Comments
1a. 1b.	S1	$NaHSO_4$ / $FeSO_4$	> 100 74[b]	0 1000	No No	25 No	No catechol Dark catechol
2.	1 & S3	none	> 100	1200	No	68	No seeds or HOOH
3.	2 & S4	$NaHSO_4$	95	200	29 56	No 56	No iron, dark No iron
4a. 4b.	3 & S5	$NaHSO_4$ / $FeSO_4$	96	20 100	34 93	no 93	Fenton Photo-Fenton
5.	S6	$NaHSO_4$ / $FeSO_4$	97	200	No	83	No HOOH
6.	4 & S7	$NaHSO_4$ / $FeSO_4$	43[b]	60	21 90	No 90	Solid seeds, Fenton Photo-Fenton
7.	S8	$NaHSO_4$ / $FeSO_4$	42[b]	40	No	97	Solid seeds, no HOOH

Notes: solar simulator lights were turned on for 60 – 90 minutes in each experiment. For control Experiment 1b, lights were turned off before catechol was added. Abbreviations: expt. = experiment, fig. = figure, RH_{max} = maximum relative humidity, $[catec.]_{peak}$ = maximum catechol concentration. **a**: seed aerosol generated from 10 mM $NaHSO_4$ solution (Experiment 3), or 10 mM $NaHSO_4$ + 67 μM $FeSO_4$ solution (Expts. 1 and 4-7). **b**: Deliquescence RH of $NaHSO_4$ is 52%, thus the seeds stayed in solid phase in Experiments 6 & 7.[25]

Results and Discussion

Results from seven experiments performed in the CESAM chamber are summarized in Table 2: 1) seed aerosol blank / dark control; 2) RH-dependent precursor wall uptake and photolysis (seed-free); and 3-7) Photolysis experiments with and without HOOH(g) as an OH radical source, with and without Fe^{2+} ions included in the seed aerosol particles, and in the presence of deliquesced or solid-phase iron-containing seed aerosol.

Table 2. Summary of results for catechol photolysis and photooxidation chamber experiments.

Expt.	Fig.	Comments	SOA_{max} ($\mu g/m^3$)	$Abs_{365,max}$	AAE	$[OH]_{(g)}$ ($\times 10^6$ molec cm^{-3})
1a.	S1	No catechol	< 3[a]	<< 0.05	3.4 ±0.1	n/a
1b.		Dark catechol	5.5	< 0.05	4.4 ±0.2	n/a
2.	1 & S3	No seeds or HOOH	37	0.36	5.3 ±0.3	1.2 ±0.6[b]
3.	2 & S4	No iron, dark	< 1	<< 0.05	1.9 ±0.1	0
		No iron	18	0.21	4.4 ±0.1	3.1 ±0.6
4a.	3 & S5	Fenton	2.4	0.025	2.8 ±0.1	1 ±1.5[b]
4b.		Photo-Fenton	20	0.27	4.8 ±0.1	5 ±3[b]
5.	S6	No HOOH	7	0.12	3.8 ±0.1	2.3 ±0.4
6.	4 & S7	Solid seeds, Fenton	< 1	< 0.05	1.5 ±0.1	9 ±2
		Photo-Fenton	15	0.18	4.6 ±0.1	7.3 ±0.3
7.	S8	Solid seeds, no HOOH	3.4	0.05	3.1 ±0.1	3.2 ±0.3

Notes: SOA_{max} = maximum quantity of secondary organic aerosol formed, as measured by ACSM. $Abs_{365,max}$ = highest recorded absorption measured at 365 nm by PILS–waveguide absorbance spectrometer with 2 m pathlength. AAE = Angstrom absorption exponent, fit to aethalometer data measured between 470 and 950 nm. n/a = no measurement. **a**: Background level of SOA formation in illuminated chamber. **b**: below measurement detection limit using loss of butanol-*d9* to quantify hydroxyl radical concentrations.

Control experiments. In Experiment 1 (Figure S1), aerosol seeds generated from a solution containing 67 μM $FeSO_4$ and 10.0 mM $NaHSO_4$ were subject to increasing RH, a cloud event, and simulated sunlight in the absence of catechol. Since $FeSO_4$ solutions absorb UV light,[26] absorption could be measured throughout the experiment by a dual-beam aethalometer. The mean AAE for the seed particles was 3.4 ±0.1 and was unaffected by changes in humidity, aerosol deliquescence (sodium bisulfate deliquesces above 52% RH),[25] or exposure to sunlight. A small amount of background SOA formation (< 3 $\mu g/m^3$) was observed during photolysis, which is attributed to trace levels of oxidant generation from contaminants present in the CESAM chamber.

An injection of 1000 ppb catechol was made into the dark, humidified chamber at the end of Experiment 1. All aerosol instruments detected catechol uptake into the aqueous phase under these conditions. The catechol parent ion signal at *m/z* 110 was prominent in ACSM spectra (Figure S2, Expt. 1). Total ACSM organic signals increased by 3.17 $\mu g/m^3$, while SMPS signals (assuming unit density) increased by 2.90 $\mu g/m^3$. These amounts match if the density of aerosol-phase catechol is 1.09 g/cm^{-3}. (Both instruments removed water during the aerosol sampling process.) Aqueous-phase catechol was also detected by PILS-waveguide spectrometer due to its absorption peak centered at ~270 nm. After catechol was taken up in the dark by deliquesced $FeSO_4$ / $NaHSO_4$ seed aerosol particles, the mean of measured Angstrom absorption exponents increased slightly from 3.4 ±0.1 to 4.4 ±0.2.

Seed-free and iron-free catechol photooxidation. In Experiment 2 (Figures 1 and S3), a large 1200 ppb catechol injection was made into the chamber in the absence of seed aerosol, and subject to increasing RH, simulated sunlight, and a dark cloud event. Gas-phase catechol PTR-

MS signals came up slowly after addition, and spiked each time water vapor was added to the chamber, and dropped when RH was increased to 99%, suggesting complex, RH-dependent interactions with the stainless steel chamber walls (and possibly also with aerosol deposited there during the prior experiment).

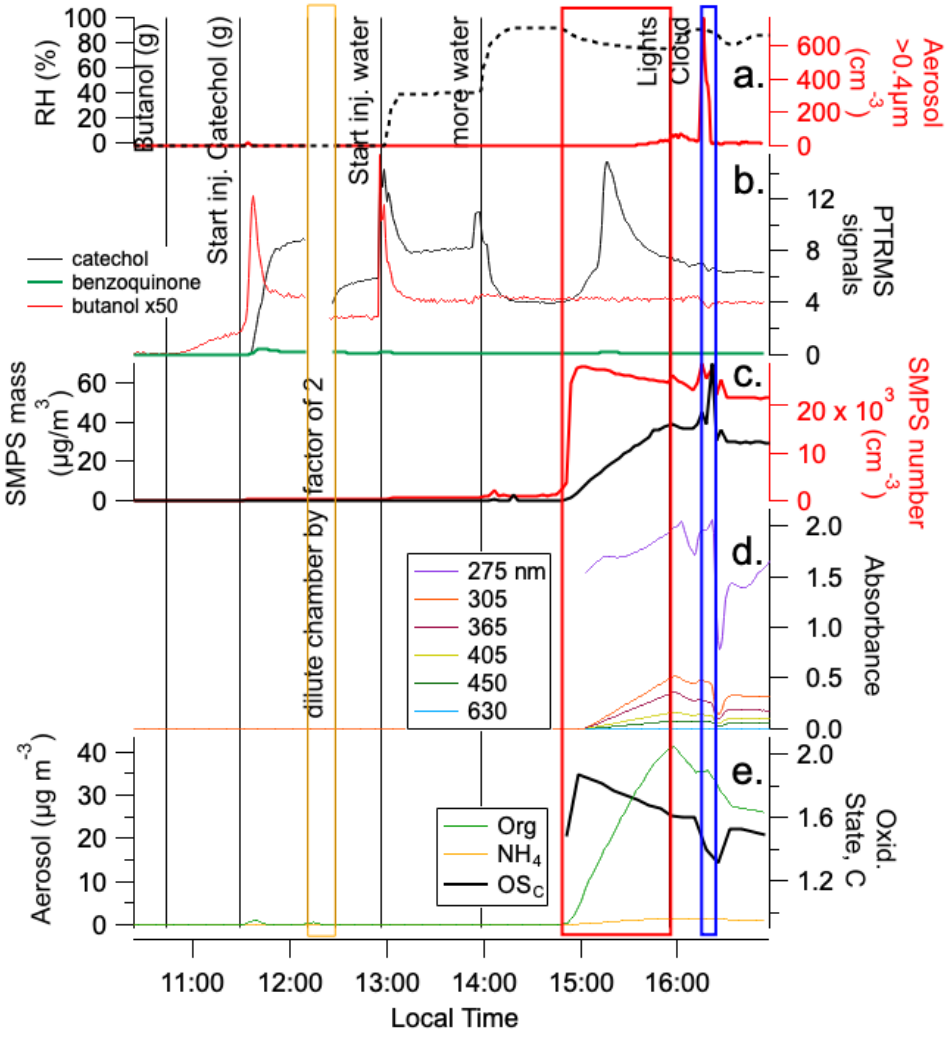

Figure 1: Experiment 2. No seeds; catechol(g), water vapor, lights, followed by dark cloud event. Between 12:10 and 12:25, half the contents in the chamber were pumped out and replaced with clean air. Panel **a**: RH (dashed line) and optical counts of aerosol particles with diameters larger than 400 nm (red, right axis). **b**: PTR-MS signals for butanol-*d9* (red, multiplied by 50),

benzoquinone (thick green line), and catechol (black line). **c**: dilution- and wall-loss-corrected SMPS aerosol mass (black) and number concentrations (red, right axis). **d**: absorbance measured in water-soluble aerosol particles by PILS / waveguide UV-vis, with absorbance below detection limit shown as flat baseline. **e**: ACSM: aerosol loadings for organic (green) and ammonium-assigned signals (orange), and oxidation state of carbon (black, right axis) .

When the lights came on in the humidified, seed-free chamber, SOA aerosol particles nucleated immediately (Figure 1 panel c), presumably triggered by the same background OH radical source that produced small amounts of SOA upon chamber illumination in Experiment 1a. Freshly nucleated particles had a carbon oxidation state (OS_C, measured by ACSM) of nearly 1.9 (Figure 1 panel e), a value far higher than that of catechol (OS_C = -0.33), indicating that early-condensing species are highly oxidized molecules. Catechol SOA was then produced continuously until the lights were turned off 70 min. later, reaching 36.6 $\mu g/m^3$ (ACSM) and 31.7 (SMPS), corresponding to an SOA dry density of 1.15 g/cm^{-3}. The OS_C declined to 1.6 during the same period, suggesting that partitioning from the gas phase of less oxidized species increased as the aqueous organic phase grew. ACSM organic ion signals between *m/z* 100 and 200 increased in a complex pattern indicative of oligomer formation, ring opening, and fragmentation occurring in the aqueous phase, with prominent peaks at *m/z* 102 (likely 4-hydroxy-2-butenoic acid, $C_4H_6O_3$),[19, 27] 116 (likely maleic acid, $C_4H_4O_4$),[19] 131, 137, 147, and 155 (Figure S2, Expt. 2).

BrC formation was detectable within 15 minutes after SOA nucleation, and aerosol absorbance increased continuously and linearly for the rest of the photolysis period, eventually reaching peaks of Abs_{365} = 0.36 (Figure 1 panel d) and AAE = 5.3 ±0.3 (Figure S3 panel f). Experiment 2

reached the highest levels of SOA formation, absorption, and AAE values, as might be expected since it involved the largest injection of catechol gas.

It is noted that gas-phase catechol PTR-MS signals climbed rapidly for the first 25 minutes after chamber lights were turned on, before declining sharply for the rest of the photolysis period (Figure 1 panel b). The source of this catechol was likely the release of catechol deposited on the humidified chamber walls earlier in Experiment 2 (since the chamber had been heated to 50°C and pumped overnight beforehand). Illumination of the CESAM chamber is always performed while the temperature control system is operating, but small increases in temperature and declines in RH are nevertheless still measurable: the chamber temperature increased from 24.6 to 25.1 C between 15:08 and 15:18, which corresponded exactly to the period of steepest increase in gas-phase catechol concentrations (Figure 1 panel b), and RH declined by 12% overall while the lights were on (Figure 1 panel a). In all other experiments with HOOH (all containing seed particles but much lower catechol levels), catechol uptake was rapid in the dark and slowed when the lights were turned on, perhaps masking a proportionally smaller release from the walls. This comparison suggests that the change from catechol release to catechol uptake observed during photolysis in Experiment 2 was likely due to depletion of wall-adsorbed catechol and to rapidly increasing rates of catechol uptake to the freshly nucleated SOA particles as they increased in mass and surface area.

As shown in Figure 1 panel c ~ e, SOA and BrC production stopped as soon as the lights were turned off in Experiment 2, indicating that SOA and BrC production are driven by reactions of radicals or by photosensitization by triplet carbon species. However, no OH radical source was added to the chamber in this experiment, and OH radical concentrations ($1.2 \pm 0.6 \times 10^6$ molec cm^{-3} measured by PTR-MS butanol-*d9* losses, Figure 1 panel b) during chamber illumination

were below the method detection limit. This suggests that the major driver of both SOA growth and BrC production was either photosensitization or the photolytic production of other radical species that do not react efficiently with butanol, such as $\bullet SO_4^-$.[28] OS_C continued to decline in the dark, but at a slower rate than in simulated sunlight. A dark cloud event at the end of the experiment did not alter any general trend.

In Experiment 3 (Figures 2 and S4), a 200 ppb catechol injection was made in the presence of dry, iron-free $NaHSO_4$ seeds. No aerosol growth was observed by either SMPS or ACSM until the seed particles were deliquesced at t = 15:26 by increasing water vapor concentrations past 52% RH (the deliquescence point of $NaHSO_4$).[25] At this point, gas-phase catechol PTR-MS signals temporarily declined by a factor of 2 within 10 min., while ACSM organic aerosol mass increased by only 0.58 $\mu g/m^3$ and SMPS mass continued to decline. The ACSM mass increase is 18% of that observed during dark catechol uptake in Experiment 1, consistent with the catechol concentration ratio (17% of Experiment 1). Addition of HOOH at t = 16:27 in the dark did not result in an observable increase in aerosol mass or BrC. No decline in gas-phase butanol-*d9* signals was observed, suggesting minimal concentrations of OH radicals were present, as expected in darkness and the absence of iron-catalyzed Fenton chemistry. However, dark HOOH addition caused rapid losses of gas-phase catechol PTR-MS signals (with a first order rate constant $k = 4.32 \pm 0.05 \times 10^{-4}$ s^{-1}), an increase in OS_C from 0.8 to 1.8 in 36 min, and an increase in PTR-MS signals for gas-phase acetic acid and acetone. The rapid loss of gas-phase catechol, increase in aerosol OS_C, and production of oxidized gases in the absence of detectable OH radicals or SOA growth together suggest that aqueous-phase oxidation of catechol by HOOH was occurring in water adsorbed on the steel chamber walls, where the reaction could be

catalyzed by iron. We hypothesize that a small amount of highly oxidized products such as acetic acid partitioned back to the aerosol, thereby increasing its OS_C.

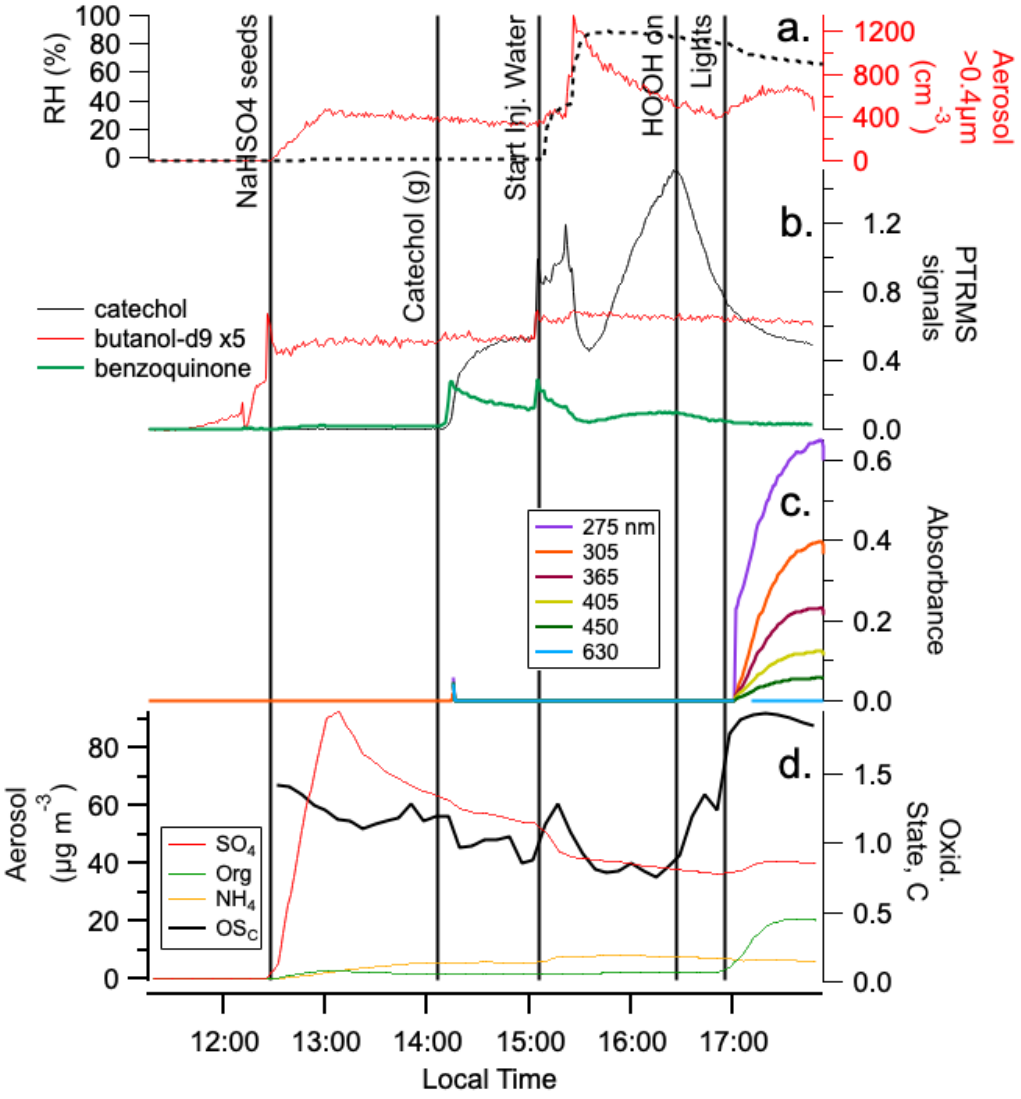

Figure 2: Experiment 3. $NaHSO_4$ seeds, catechol(g), water vapor, HOOH, and lights. Panel **a**: RH (dashed line) and optical counts of aerosol particles with diameters larger than 400 nm (red, right axis). **b**: PTR-MS signals for butanol-*d9* (red, multiplied by 5), benzoquinone (thick green line), and catechol (black). **c**: absorbance measured in water-soluble aerosol particles by PILS / waveguide UV-vis, with absorbance below detection limit shown as flat baseline. **d**: average

oxidation state of carbon (thick black line) and ACSM aerosol loadings, before (solid) and after (dashed) dilution corrections, for sulfate (red), organic (green), and ammonium-assigned signals (orange).

Once the lights were turned on, however, rapid formation of 18 μg/m^3 SOA was observed (Figure 2 panel d), and the OH radical concentrations inferred from butanol-*d9* losses increased from zero to [OH] = 3.1 ±0.6 ×10^6 molec cm^{-3}, as expected given the presence of HOOH gas as an OH precursor. The ACSM mass spectral peaks assigned to organic species had the same prominent peaks observed as in Experiment 2 when catechol was photolyzed without oxidant or seed particles present (Figure S2). The SOA formed was again brown, with similar mass absorption coefficients (1.7 m^2 g^{-1}) and Angstrom absorption exponents (4.4 ±0.1) in both experiments. Maximum SOA concentrations were reached in 43 min, while maximum BrC absorbance took slightly longer to achieve (55 min., Figure 2 panels c and d). In terms of integrated gas-phase OH concentrations, these times are equivalent to 2.2 and 2.8 h of atmospheric oxidation where [OH] = 1×10^6 molec cm^{-3}. These observations suggest that catechol oxidation by OH radicals (from HOOH photolysis) and by photosensitization triggers the formation of similar BrC products, at least for the first few hours of photooxidation under ambient conditions.

Aqueous catechol photooxidation with Fenton and photo-Fenton chemistry. Experiment 4 (Figures 3 and S5) repeated Experiment 3 but with the addition of 67 μM $FeSO_4$ to the 10 mM $NaHSO_4$ seed aerosol solution, enabling the dark generation of OH radicals via Fenton chemistry once HOOH is added. The product Fe^{3+} can be reduced back to Fe^{2+} in a one-electron redox reaction with catechol,[29] allowing continued oxidant generation while also producing semiquinone radicals and quinones which are prone to oligomer formation.[20] Alternatively, catechol-iron

complexes can catalyze hydroxyl group transfer reactions between HOOH and organic species.[30] In Experiment 4, 2.4 μg/m^3 of SOA was generated when HOOH(g) was added to the dark, humidified chamber containing catechol and Fe^{2+}-containing seeds. For comparison, in the absence of Fe^{2+} (Experiment 3), no dark SOA production was observed upon HOOH addition, even though catechol concentrations were 10× higher. The OS_C in Experiment 4 increased from 0.8 to 1.8 in 15 min., more than twice the rate of increase in the absence of Fe^{2+}. A small amount of BrC absorbance was observed by PILS/waveguide and aethalometer instruments, and butanol-*d9* levels declined slightly, indicating the presence of •OH in the gas phase; neither of these occurred in the dark in the absence of Fe^{2+}. The observed enhancement in SOA generation and more rapid oxidation of SOA material are expected results of oxidant generation by aqueous-phase Fenton chemistry. Gas-phase concentrations of a species detected by PTR-MS at *m/z* 109, likely *1,2*-benzoquinone (the oxidation product of catechol), increased by 70% upon dark HOOH addition in Experiment 4, but not Experiment 3. This is direct evidence that dark redox reactions between catechol and Fe^{3+} (produced by the Fenton reaction) are occurring.

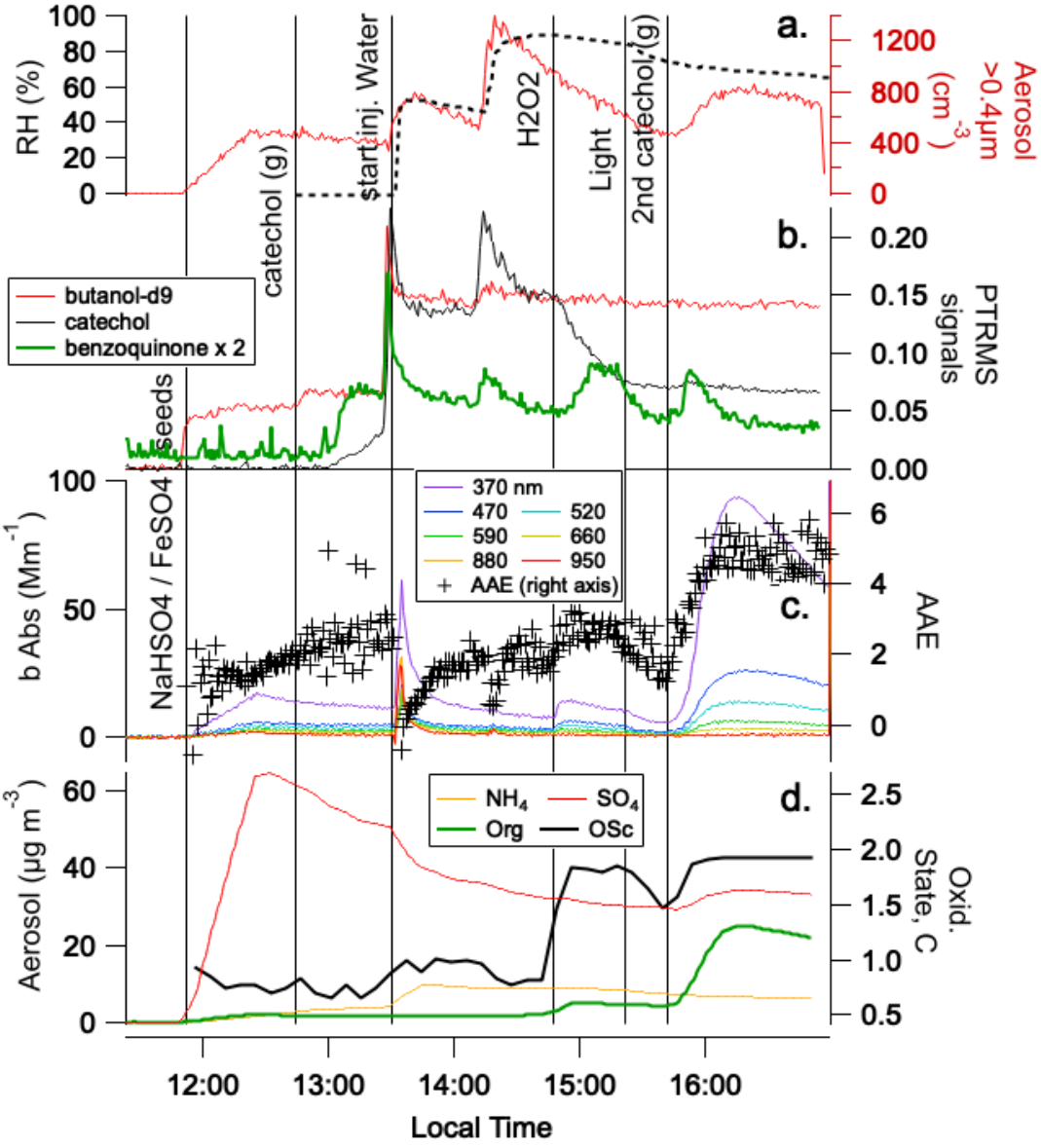

Figure 3: Experiment 4. $NaHSO_4$ / $FeSO_4$ seeds, catechol(g), water vapor, HOOH, lights, and additional catechol(g). Panel **a**: RH (dashed line) and optical counts of aerosol particles with diameters larger than 400 nm (red, right axis). **b**: PTR-MS signals for butanol-*d9* (red), catechol (black line), and benzoquinone (thick green line, ×2). **c**: aerosol absorptivity and Angstrom absorption exponents (+) measured by 7-wavelength aethalometer. **d**: average oxidation state of carbon (thick black line) and ACSM aerosol loadings, before (solid) and after (dashed) dilution corrections, for sulfate (red), organic (green), and ammonium-assigned signals (orange).

Fe^{3+} can also be reduced back to Fe^{2+} by photolysis, enabling photo-Fenton chemistry. Once the lights were turned on (and gas-phase catechol was replenished by a second addition to the chamber), 20 μg/m^3 of SOA was produced with a similar Angstrom absorption coefficient, organic mass spectrum, and brownness as SOA produced during photolysis in Experiments 2 and 3, even though less catechol was added to the chamber. Inferred gas-phase OH levels were 6 times lower than in iron-free Experiment 3, however, even as maximum SOA and BrC levels were reached in 30 min. instead of an hour or more. The quick production of SOA and BrC suggest that photo-Fenton chemistry with iron and HOOH enhanced aqueous-phase OH radical production, reacting with catechol to more rapidly form SOA and BrC, and then more quickly proceeding to destroy SOA and BrC through further oxidation reactions. The lower levels of gas-phase OH radicals compared to Experiment 3 were likely caused by a depletion of gas-phase HOOH due to enhanced aqueous-phase losses of HOOH. This observation also confirms that OH radicals generated in the aqueous phase are too reactive to escape to the gas phase.

Catechol photooxidation in the presence of Fe^{2+} ions. Experiment 5 (Figure S6) was conducted with iron-containing seeds but no HOOH present. This may allow insoluble catechol polymers to form, especially if the aerosol is acidic,[10] but Fenton chemistry cannot take place in the aerosol. In the 80 minutes after the chamber lights were turned on, 7 μg/m^3 SOA was generated with OS_C reaching 1.8 again. Gas-phase OH radical concentrations inferred from butanol-d9 losses were detectable ([OH] = 2.3 ±0.4 ×10^6 molec cm^{-3}), comparable to Experiment 3 where HOOH was photolyzed. This suggests that triplet carbon species (photosensitizers) are being formed and reacting with dissolved oxygen to efficiently generate OH radicals, which are, unlike in Experiment 4, somehow able to influence gas phase OH concentrations. The difference may be

that photo-Fenton chemistry occurs in the full volume of aqueous aerosol particles, making aqueous OH radical reactions overwhelmingly more likely than transfer to the gas phase, while catechol photosensitization may occur preferentially at the air-water interface where such transfer might be possible. Photosensitization at the air-water interface would be consistent with the known surface activity of catechol.[19] Furthermore, surface-adsorbed phenolic species have red-shifted absorption spectra,[31] enhancing absorption of solar radiation and therefore photosensitization at droplet surfaces.

Water-soluble aerosol absorbance at 365 nm measured by PILS-waveguide reached 0.13 and was still increasing after 80 minutes in Experiment 5. In terms of integrated gas-phase OH exposure, this is the equivalent of 3.3 h of atmospheric OH oxidation. The SOA produced in Experiment 5 was quantitatively similar to that of previous experiments in terms of brownness (MAC_{365}), mass spectrum, and oxidation level. However, the ratio of BrC formation to catechol levels was double that of Experiment 2, suggesting a measurable enhancement of BrC formation due to the presence of Fe^{2+}, but only in sunlight. Dark BrC formation was not observed in Experiment 5, likely due to lack of the particle-phase acidity required for direct catechol – iron oligomer-forming reactions.[10]

Catechol photooxidation with non-deliquesced seed aerosol. In Experiment 6 (Figures 4 and S7), 60 ppb of catechol gas was photooxidized in the presence of HOOH(g) and undeliquesced (solid phase) 10 mM $NaHSO_4$ / 61 μM $FeSO_4$ aerosol seeds at 41% RH. Without an aqueous phase present like in Experiment 4, one would expect dark OH production by Fenton chemistry to be shut down. Instead, the dark portion of Experiment 6 had the highest *gas-phase* OH radical concentration measured in any experiment ([OH] = 9 ±2 $\times 10^6$ molec cm^{-3} inferred from PTR-MS butanol-*d9* signals), the highest loss rates of gas-phase catechol (k = 4.9 ±0.2 $\times 10^{-4}$ s^{-1}) and the

highest production of benzoquinone product (gas phase PTR-MS signals at *m/z* 109 increased by more than a factor of 8). These observations indicate that Fenton chemistry was actively occurring in surface-adsorbed water layers, below the deliquescence RH of $NaHSO_4$ (52%).[25] They also suggest that benzoquinone and possibly OH radicals, once formed in these surface water layers, could more easily escape to the gas phase than in Experiment 4 with deliquesced seeds. Rapid loss of benzoquinone to the gas phase may be the reason that no aqueous-phase BrC or SOA production was detected in the dark portion of Experiment 6, in spite of the evidence that oxidation was occurring.

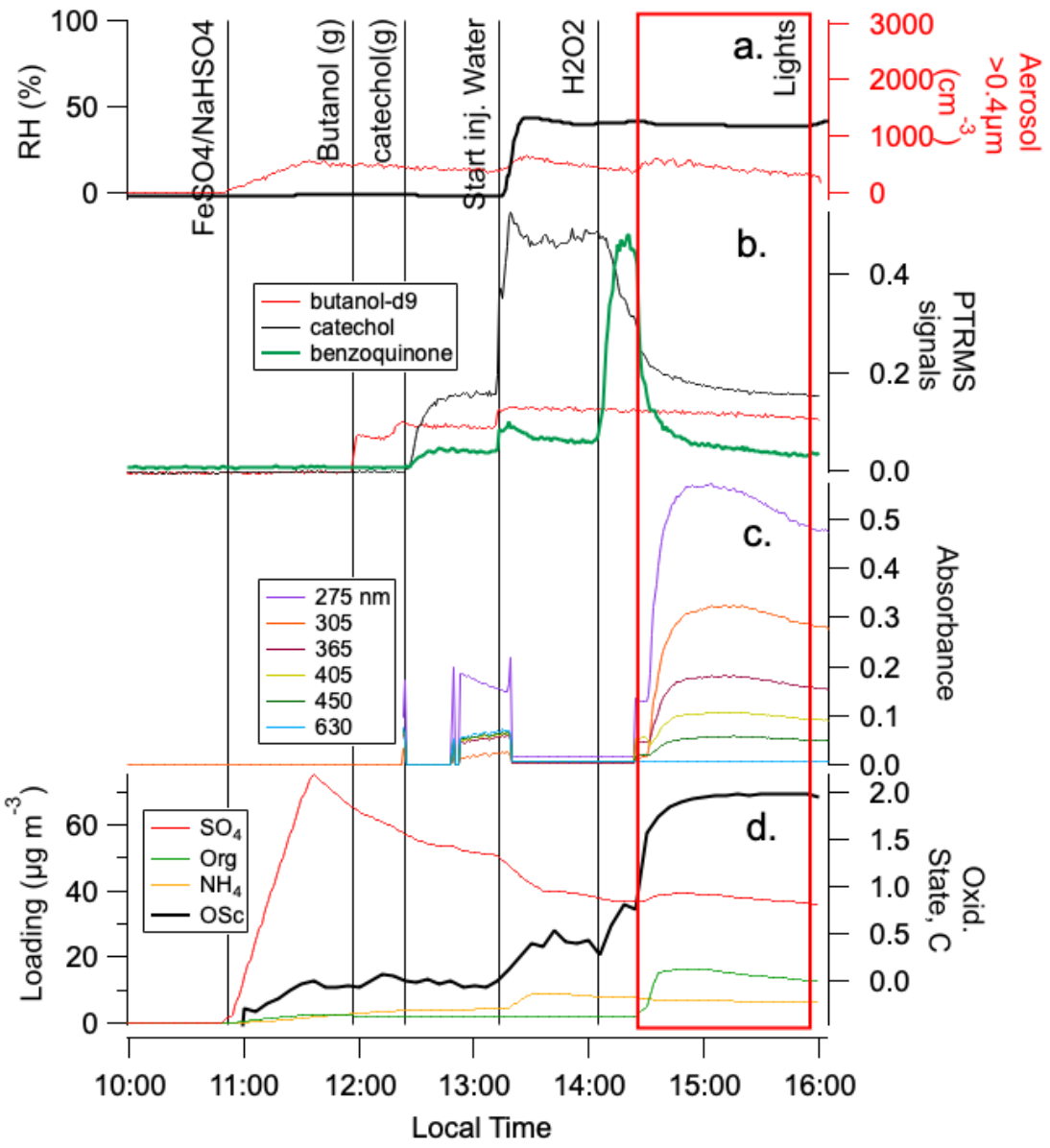

Figure 4: Experiment 6. $NaHSO_4$ / $FeSO_4$ seeds, catechol(g), water vapor, HOOH(g), and lights. Panel **a**: RH (dashed line) and optical counts of aerosol particles with diameters larger than 400 nm (red, right axis). **b**: PTR-MS signals for butanol-*d9* (red), catechol (black line). and benzoquinone (thick green line). **c**: absorbance measured in water-soluble aerosol particles by PILS / waveguide UV-vis, with absorbance below detection limit shown as flat baseline. **d**: average oxidation state of carbon (thick black line, right axis) and dilution-corrected ACSM aerosol loadings for sulfate (red), organic (green), and ammonium -assigned signals (orange).

Once the lights were turned on in Experiment 6, 15 μg/m^3 of light-absorbing SOA was formed within 20 minutes, after which aerosol absorbance and SOA levels declined. In terms of integrated gas-phase OH levels, this time to maximum BrC corresponds to 2.8 h of atmospheric oxidation at [OH] = 1 ×10^6 molec cm^{-3}. The was no detectable delay between the onset of SOA and BrC production (≤ 3 min, near the 1 min chamber mixing time and smaller than the 3 min time step of SMPS measurements). The freshly-generated catechol SOA had an OS_C = 1.6, increasing to 2.0 within 35 min. This highly oxygenated SOA may have condensed along with substantial water vapor, or depressed the deliquescence point of the seed particles below 52% RH, such that aqueous-phase BrC formation chemistry could commence at RH levels between 38 and 41%. With the lights on and HOOH(g) present, OH radical levels (inferred from PTR-MS butanol-*d9* losses) would be expected to increase over what was measured in the dark, but instead they declined slightly to [OH] = 7.3 ±0.3 ×10^6 molec cm^{-3}. This decline in gas-phase OH radical concentrations suggests that aqueous photo-Fenton chemistry is now occurring in a greater aerosol volume, not just in surface-adsorbed water. OH radicals produced by photo-Fenton chemistry therefore no longer have any chance to escape to the gas phase, offsetting the addition of gas-phase OH production by HOOH photolysis. The amount of SOA and BrC formed in Experiment 6, relative to the amount of catechol added to the chamber, was the highest of any experiment. This likely indicates that a small amount of aerosol-phase water, saturated with iron, is a more efficient reactor for catechol photooxidation than more dilute aqueous aerosol particles or cloud droplets present at higher RH levels.

In Experiment 7 (Figure S8), iron-containing $NaHSO_4$ seeds were kept below deliquescence again, exposed to 40 ppb catechol gas, and photolyzed, but this time without HOOH. Under these

conditions, only a small amount of highly oxidized and light-absorbing SOA formed in the illuminated chamber, with amounts barely in excess of detection limits (only 3.4 μg/m^3 of SOA and Abs_{365} = 0.05 after 90 min.). OS_C reached 1.9 after 50 minutes of photolysis. Inferred gas-phase OH radical concentrations were 3.2 ±0.3 ×10^6 molec cm^{-3}, only 38% higher than those in Experiment 5, where particles were deliquesced. The similarity in OH production from deliquesced droplets and solid particles with surface-adsorbed water in HOOH-free experiments suggests that OH radicals in both experiments were likely formed by photosensitization at the aerosol surface, and thus could sometimes escape to the gas phase. No such similarity was observed between experiments at different RH levels with HOOH present (*e.g.* Experiments 4 and 6). These comparisons again support the idea that OH production from catechol photosensitization occurs at the air-water interface, but Fenton and photo-Fenton chemistry occurs throughout the aqueous phase.

Atmospheric Implications

Overall, in Experiments 2-7 BrC and SOA were produced in sunlight whether or not HOOH was present, albeit at a faster rate when HOOH was present. In both cases, BrC formation can be attributed to OH oxidation of catechol in the aqueous aerosol phase. HOOH photolysis, and in the absence of HOOH, surface-enhanced catechol photosensitization, both served as significant sources of OH radicals. As one might expect from a system where all BrC and SOA appear to be produced by catechol + •OH reactions, BrC production measured as absorption at 365 nm was proportional to SOA formation in all experiments with catechol, as summarized in Figure 5, R^2 = 0.97). This resulted in a similar MAC_{365} value for SOA produced in all catechol experiments of 1.7 ±0.2 m^2 g^{-1}, with no significant dependence on the addition of HOOH or even iron. However,

Experiments 4b and 6, performed with soluble iron and HOOH, produced the most SOA and BrC per added catechol. Thus, it appears that the major role of soluble iron and HOOH with regard to BrC formation in these experiments is to serve as an additional source of OH radicals via photo-Fenton chemistry. We do not observe strong evidence of a different, iron-specific mechanism by which catechol forms BrC.

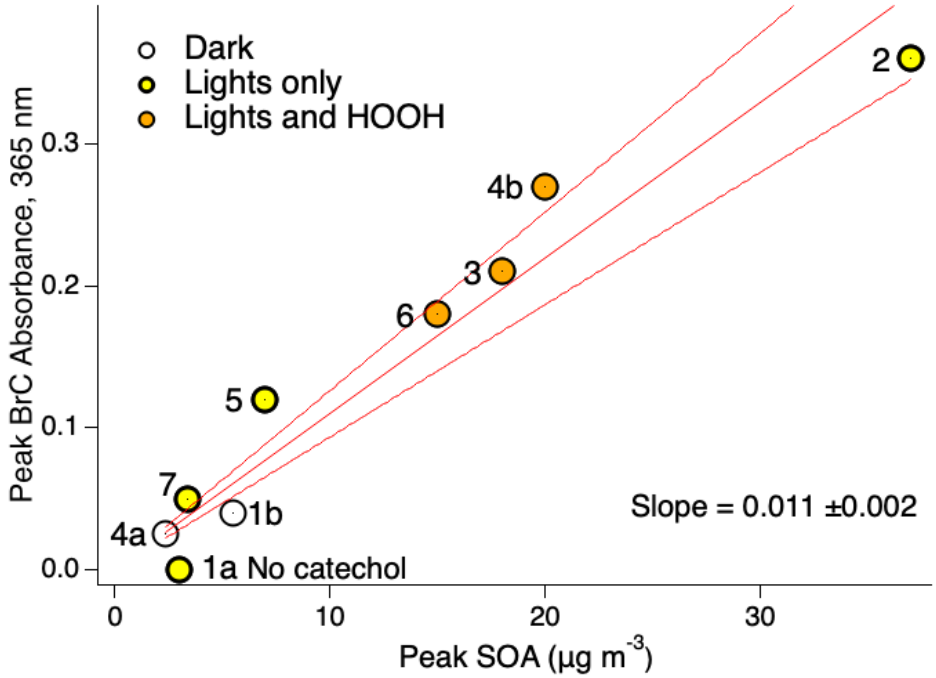

Figure 5: Summary of peak water-soluble aerosol absorption measured by PILS / waveguide UV/vis spectrometer at 365 nm, as a function of peak SOA level measured by ACSM. Symbol colors designate reaction conditions: dark run (white); lights + HOOH (orange); lights only (yellow). Each symbol is labelled with its experiment number. Experiment 1a did not include catechol. Experiments 1 and 4-7 contained trace levels of $FeSO_4$ in the seed particle material, while 2-3 were iron-free. Using the slope of least squares y = mx fit line (shown with its 95% confidence intervals) to calculate an average MAC_{365} value for all experiments with catechol results in MAC_{365} for catechol SOA = 1.7 ±0.2 $m^2\ g^{-1}$.

Typical iron(III) concentrations in clouds and aerosol have been estimated at ~10^{-6} and 10^{-2} M, respectively.[4] The 67 uM $FeSO_4$ component of solutions used to generate aqueous aerosol in Experiments 1 and 4-7 was appropriately in the middle of that range, and are expected to quickly generate Fe^{3+} via oxidation, especially in the presence of HOOH. Similarly, the concentrations of dihydroxybenzenes in smoke plumes range up to 50 ppb,[32] overlapping the lower end of catechol concentrations used in this study. While off-gassing from the humidified chamber walls served as a source of catechol, especially in Experiment 2, we note that catechol is produced in smoke plumes by the oxidation of phenol. The conditions used in these experiments were similar enough to those of a smoke plume that measured SOA and BrC formation rates can be compared with atmospheric observations using the concept of integrated OH exposure. In Experiments 6 and 7, where gas-phase OH levels were above the limit of quantitation (10× noise), peak BrC formation by catechol was reached at integrated gas-phase OH exposures corresponding to 3 and >5 h of atmospheric photooxidation. Thus, we conclude that photooxidation of catechol could contribute to the production of BrC in smoke plumes for the first few hours of aging, as has been observed in several lab and field studies.[33, 34]

The MAC_{365} values (1.7 ±0.2 m^2 g^{-1}) and AAE values (3.1 to 5.3) measured in this study for catechol SOA place it squarely in the category of "medium BrC" using the BrC categories of Saleh *et al*.,[35, 36] which is typical of BrC emissions from high-temperature biomass burning, but not of secondary BrC from smoldering biomass. Thus, even though the BrC produced from catechol photooxidation in this study is secondary (generated from gas-phase reactants), it is intensely brown. However, in a real smoke plume, catechol SOA would be diluted by the condensation of many other organic species that are both less reactive and less light-absorbing. Because catechol is abundant in biomass burning emissions, highly reactive due to its *ortho*-hydroxyphenol

structure, and able to efficiently form SOA and BrC via OH photooxidation, the evidence from this work is consistent with catechol being a major source of secondary BrC and SOA in smoke plumes.

ASSOCIATED CONTENT

Supporting Information.

The following files are available free of charge. Summary graphs for Experiments 1-7, and a comparison of ACSM organic component mass spectra from Experiments 1-7. (PDF)

AUTHOR INFORMATION

Corresponding Author

*David De Haan, Department of Chemistry and Biochemistry, University of San Diego, 5998 Alcala Park, San Diego CA 92110, USA. ddehaan@sandiego.edu

ACKNOWLEDGMENT

This work was funded by NSF grants AGS-1826593 and AGS-2218491. CNRS-INSU is gratefully acknowledged for supporting CESAM as an open facility through the National Instrument label. This project/work has received funding from the European Union's Horizon 2020 research and innovation programme through the EUROCHAMP-2020 Infrastructure Activity under grant agreement No 730997. AERIS/ACTRIS is acknowledged for supporting the Eurochamp data center.

DATA AVAILABILITY

Concentration-time profiles for the CESAM chamber experiments are freely accessible in .edf format through the chamber database at data.eurochamp.org maintained by AERIS for the benefit of ACTRIS ERIC. (Expt. 1: https://doi.org/10.25326/DKDW-D669. Expt. 2: https://doi.org/10.25326/KBD6-8C07. Expt. 3: https://doi.org/10.25326/10VG-F343. Expt. 4: https://doi.org/10.25326/JWBX-F269. Expt. 5: https://doi.org/10.25326/1RJS-QW25. Expt. 6: https://doi.org/10.25326/Z5P7-W082. Expt. 7: https://doi.org/10.25326/D5DQ-D858.)

ABBREVIATIONS

BrC, brown carbon; HOOH, hydrogen peroxide; OH, hydroxyl radical; MAC_{365}, mass absorption coefficient measured at 365 nm; SOA, secondary organic aerosol; CESAM, chamber for experimental multiphase atmospheric simulation; RH, relative humidity; PTR-MS, proton transfer reaction mass spectrometer; FTIR, Fourier transform infrared spectroscopy; PILS, particle into liquid sampling; ACSM, aerosol chemical speciation; SMPS, scanning mobility particle sizing; catec., catechol; AAE, Angstrom absorption exponent; OS_C, oxidation state of carbon.

REFERENCES

1. Palm, B. B.; Peng, Q.; Fredrickson, C. D.; Lee, B. H.; Garofalo, L. A.; Pothier, M. A.; Kreidenweis, S. M.; Farmer, D. K.; Pokhrel, R. P.; Shen, Y.; Murphy, S. M.; Permar, W.; Hu, L.; Campos, T. L.; Hall, S. R.; Ullmann, K.; Zhang, X.; Flocke, F.; Fischer, E. V.; Thornton, J. A., Quantification of organic aerosol and brown carbon evolution in fresh wildfire plumes. *Proceedings of the National Academy of Sciences* **2020,** *117*, (47), 29469-29477. doi:10.1073/pnas.2012218117
2. Chang, J. L.; Thompson, J. E., Characterization of colored products formed during irradiation of solutions containing H_2O_2 and phenolic compounds. *Atmos. Environ.* **2010,** *44*, 541-551. doi:10.1016/j.atmosenv.2009.10.042

3. Yu, L.; Smith, J.; Laskin, A.; Anastasio, C.; Laskin, J.; Zhang, Q., Chemical characterization of SOA formed from aqueous-phase reactions of phenols with the triplet excited state of carbonyl and hydroxyl radical. *Atmos. Chem. Phys.* **2014,** *14*, (24), 13801-13816. doi:10.5194/acp-14-13801-2014
4. Chin, H.; Hopstock, K. S.; Fleming, L. T.; Nizkorodov, S. A.; Al-Abadleh, H. A., Effect of aromatic ring substituents on the ability of catechol to produce brown carbon in iron(iii)-catalyzed reactions. *Environmental Science: Atmospheres* **2021,** *1*, (2), 64-78. doi:10.1039/D0EA00007H
5. Zhang, J.; Shrivastava, M.; Ma, L.; Jiang, W.; Anastasio, C.; Zhang, Q.; Zelenyuk, A., Modeling Novel Aqueous Particle and Cloud Chemistry Processes of Biomass Burning Phenols and Their Potential to Form Secondary Organic Aerosols. *Environ Sci Technol* **2024,** *58,* (8), 3776-3786. doi:10.1021/acs.est.3c07762
6. Arciva, S.; Ma, L.; Mavis, C.; Guzman, C.; Anastasio, C., Formation and Loss of Light Absorbance by Phenolic Aqueous SOA by OH and an Organic Triplet Excited State. *EGUsphere* **2023,** *2023*, 1-24. doi:10.5194/egusphere-2023-2719
7. Palm, B. B.; Peng, Q.; Fredrickson, C. D.; Lee, B. H.; Garofalo, L. A.; Pothier, M. A.; Kreidenweis, S. M.; Farmer, D. K.; Pokhrel, R. P.; Shen, Y.; Murphy, S. M.; Permar, W.; Hu, L.; Campos, T. L.; Hall, S. R.; Ullmann, K.; Zhang, X.; Flocke, F.; Fischer, E. V.; Thornton, J. A., Quantification of organic aerosol and brown carbon evolution in fresh wildfire plumes. *Proceedings of the National Academy of Sciences* **2020,** *117*, (47), 29469. doi:10.1073/pnas.2012218117
8. Broere, D. L. J.; Plessius, R.; van der Vlugt, J. I., New avenues for ligand-mediated processes – expanding metal reactivity by the use of redox-active catechol, o-aminophenol and o-phenylenediamine ligands. *Chem. Soc. Rev.* **2015,** *44*, (19), 6886-6915. doi:10.1039/C5CS00161G
9. Yang, J.; Cohen Stuart, M. A.; Kamperman, M., Jack of all trades: versatile catechol crosslinking mechanisms. *Chem. Soc. Rev.* **2014,** *43*, (24), 8271-8298. doi:10.1039/C4CS00185K
10. Slikboer, S.; Grandy, L.; Blair, S. L.; Nizkorodov, S. A.; Smith, R. W.; Al-Abadleh, H. A., Formation of Light Absorbing Soluble Secondary Organics and Insoluble Polymeric Particles from the Dark Reaction of Catechol and Guaiacol with Fe(III). *Environ Sci Technol* **2015,** *49*, (13), 7793-7801. doi:10.1021/acs.est.5b01032
11. Shultz, D. A.; Hollomon, M. G., Preparation and EPR Spectroscopic Investigation of Conjugated Oligomers Containing Semiquinone Repeat Units. *Chemistry of Materials* **2000,** *12*, (2), 580-585. doi:10.1021/cm9907155
12. Powell, H. K. J.; Taylor, M. C., Interactions of iron(II) and iron(III) with gallic acid and its homologues: a potentiometric and spectrophotometric study. *Australian Journal of Chemistry* **1982,** *35*, (4), 739-756. doi:10.1071/CH9820739
13. Qin, L.; Yang, L.; Yang, J.; Weber, R.; Ranguelova, K.; Liu, X.; Lin, B.; Li, C.; Zheng, M.; Liu, G., Photoinduced formation of persistent free radicals, hydrogen radicals, and hydroxyl radicals from catechol on atmospheric particulate matter. *iScience* **2021,** *24*, (3), 102193. doi:https://doi.org/10.1016/j.isci.2021.102193
14. Olariu, R. I.; Barnes, I.; Becker, K. H.; Klotz, B., Rate coefficients for the gas-phase reaction of OH radicals with selected dihydroxybenzenes and benzoquinones. *Intl. J. Chem. Kinet.* **2000,** *32*, (11), 696-702. doi:https://doi.org/10.1002/1097-4601(2000)32:11<696::AID-KIN5>3.0.CO;2-N

15. Zein, A. E.; Coeur, C.; Obeid, E.; Lauraguais, A.; Fagniez, T., Reaction Kinetics of Catechol (1,2-Benzenediol) and Guaiacol (2-Methoxyphenol) with Ozone. *The Journal of Physical Chemistry A* **2015,** *119*, (26), 6759-6765. doi:10.1021/acs.jpca.5b00174
16. Hoffmann, E. H.; Tilgner, A.; Wolke, R.; Böge, O.; Walter, A.; Herrmann, H., Oxidation of substituted aromatic hydrocarbons in the tropospheric aqueous phase: kinetic mechanism development and modelling. *Phys. Chem. Chem. Phys.* **2018,** *20*, (16), 10960-10977. doi:10.1039/C7CP08576A
17. Jaber, S.; Lallement, A.; Sancelme, M.; Leremboure, M.; Mailhot, G.; Ervens, B.; Delort, A. M., Biodegradation of phenol and catechol in cloud water: comparison to chemical oxidation in the atmospheric multiphase system. *Atmos. Chem. Phys.* **2020,** *20*, (8), 4987-4997. doi:10.5194/acp-20-4987-2020
18. Gurol, M. D.; Nekouinaini, S., Kinetic behavior of ozone in aqueous solutions of substituted phenols. *Industrial & Engineering Chemistry Fundamentals* **1984,** *23*, (1), 54-60. doi:10.1021/i100013a011
19. Pillar-Little, E. A.; Camm, R. C.; Guzman, M. I., Catechol Oxidation by Ozone and Hydroxyl Radicals at the Air–Water Interface. *Environ Sci Technol* **2014,** *48*, (24), 14352-14360. doi:10.1021/es504094x
20. Sánchez-Cortés, S.; Francioso, O.; García-Ramos, J. V.; Ciavatta, C.; Gessa, C., Catechol polymerization in the presence of silver surface. *Colloids and Surfaces A: Physicochemical and Engineering Aspects* **2001,** *176*, (2), 177-184. doi:https://doi.org/10.1016/S0927-7757(00)00630-0
21. Pinnataip, R.; Lee, B. P., Oxidation Chemistry of Catechol Utilized in Designing Stimuli-Responsive Adhesives and Antipathogenic Biomaterials. *ACS Omega* **2021,** *6*, (8), 5113-5118. doi:10.1021/acsomega.1c00006
22. Wang, J.; Doussin, J. F.; Perrier, S.; Perraudin, E.; Katrib, Y.; Pangui, E.; Picquet-Varrault, B., Design of a new multi-phase experimental simulation chamber for atmospheric photosmog, aerosol and cloud chemistry research. *Atmos. Meas. Tech.* **2011,** *4*, 2465-2494. doi:10.5194/amt-4-2465-2011
23. Barmet, P.; Dommen, J.; DeCarlo, P. F.; Tritscher, T.; Praplan, A. P.; Platt, S. M.; Prévôt, A. S. H.; Donahue, N. M.; Baltensperger, U., OH clock determination by proton transfer reaction mass spectrometry at an environmental chamber. *Atmos. Meas. Tech.* **2012,** *5*, (3), 647-656. doi:10.5194/amt-5-647-2012
24. Ródenas, M. *IR spectrum: 1,2-Dihydroxybenzene - Catechol - Pyrocatechol* (Version 1.0) [Data set]. AERIS. **2017.** https://doi.org/10.25326/BVGF-SM17
25. Pilinis, C.; Seinfeld, J. H., Continued development of a general equilibrium model for inorganic multicomponent atmospheric aerosols. *Atmospheric Environment (1967)* **1987,** *21*, (11), 2453-2466. doi:https://doi.org/10.1016/0004-6981(87)90380-5
26. Szilágyi, I.; Königsberger, E.; May, P. M., Spectroscopic characterisation of weak interactions in acidic titanyl sulfate–iron(ii) sulfate solutions. *Dalton Transactions* **2009**, (37), 7717-7724. doi:10.1039/B906803A
27. Lasovsky, J.; Hrbac, J.; Sichertova, D.; Bednar, P., Oxidation and chemiluminescence of catechol by hydrogen peroxide in the presence of Co(II) ions and CTAB micelles. *Luminescence* **2007,** *22*, (5), 501-506. doi:https://doi.org/10.1002/bio.995
28. Cope, J. D.; Bates, K. H.; Tran, L. N.; Abellar, K. A.; Nguyen, T. B., Sulfur radical formation from the tropospheric irradiation of aqueous sulfate aerosols. *Proceedings of the National Academy of Sciences* **2022,** *119*, (36), e2202857119. doi:10.1073/pnas.2202857119

29. Romero, R.; Contreras, D.; Sepúlveda, M.; Moreno, N.; Segura, C.; Melin, V., Assessment of a Fenton reaction driven by insoluble tannins from pine bark in treating an emergent contaminant. *J Hazard Mater* **2020,** *382*, 120982. doi:https://doi.org/10.1016/j.jhazmat.2019.120982
30. Hamilton, G. A.; Friedman, J. P., A Hydroxylation of Anisole by Hydrogen Peroxide Requiring Catalytic Amounts of Ferric Ion and Catechol. *J. Am. Chem. Soc.* **1963,** *85*, (7), 1008-1009. doi:10.1021/ja00890a044
31. Bononi, F. C.; Chen, Z.; Rocca, D.; Andreussi, O.; Hullar, T.; Anastasio, C.; Donadio, D., Bathochromic Shift in the UV–Visible Absorption Spectra of Phenols at Ice Surfaces: Insights from First-Principles Calculations. *The Journal of Physical Chemistry A* **2020,** *124*, (44), 9288-9298. doi:10.1021/acs.jpca.0c07038
32. Pillar-Little, E. A.; Zhou, R.; Guzman, M. I., Heterogeneous Oxidation of Catechol. *The Journal of Physical Chemistry A* **2015,** *119*, (41), 10349-10359. doi:10.1021/acs.jpca.5b07914
33. Schnitzler, E. G.; Liu, T.; Hems, R.; Abbatt, J., Emerging investigator series: Heterogeneous OH oxidation of primary brown carbon aerosol: effects of relative humidity and volatility. *Environmental Science: Processes & Impacts* **2020,** *22*, 2162-2171. doi:10.1039/D0EM00311E
34. Zeng, L.; Dibb, J.; Scheuer, E.; Katich, J. M.; Schwarz, J. P.; Bourgeois, I.; Peischl, J.; Ryerson, T.; Warneke, C.; Perring, A. E.; Diskin, G. S.; DiGangi, J. P.; Nowak, J. B.; Moore, R. H.; Wiggins, E. B.; Pagonis, D.; Guo, H.; Campuzano-Jost, P.; Jimenez, J. L.; Xu, L.; Weber, R. J., Characteristics and evolution of brown carbon in western United States wildfires. *Atmos. Chem. Phys.* **2022,** *22*, (12), 8009-8036. doi:10.5194/acp-22-8009-2022
35. Saleh, R., From Measurements to Models: Toward Accurate Representation of Brown Carbon in Climate Calculations. *Current Pollution Reports* **2020,** *6*, (2), 90-104. doi:10.1007/s40726-020-00139-3
36. Siemens, K.; Morales, A.; He, Q.; Li, C.; Hettiyadura, A. P. S.; Rudich, Y.; Laskin, A., Molecular Analysis of Secondary Brown Carbon Produced from the Photooxidation of Naphthalene. *Environ Sci Technol* **2022,** *56*, (6), 3340-3353. doi:10.1021/acs.est.1c03135

TOC ART